Aust. J. Phys., 1985, **38**, 41–62

The Dynamics of Steady Hexagonal Magnetoconvection

J. O. Murphy and J. M. Lopez

Department of Mathematics, Monash University,
Clayton, Vic. 3168.

Abstract

The dynamic interaction between an initially uniform vertical magnetic field and a Rayleigh–Benard type layer of convecting fluid is investigated under steady-state conditions. Particular attention is given to the roles of the diffusivities in determining the extent to which a magnetic field is induced and convective motions inhibited. The model demonstrates how the perturbed magnetic field is generated at the base of the convection zone, which is a region of converging fluid flow, and is expelled from regions of divergent flow.

1. Introduction

Theoretical investigation of the interaction between magnetic fields and buoyancy-driven thermal convection in electrical conducting fluids has attracted a great deal of interest and attention over the past couple of decades, due in the main to the phenomena of sunspots and other large scale magnetic activities in the Sun. More recently additional interest has been generated due to the ability of solar observers, employing new techniques, to resolve features on the scale of a few hundred kilometres, revealing previously undetected small scale magnetic structures interacting with granular convection.

Initial studies (Chandrasekhar 1961; Danielson 1961) were restricted to the linear case, and experimental studies (Nakagawa 1957, 1959) only dealt with establishing parameter values at the marginal states, which are described also by the linear theory. Undoubtedly, such investigations have led to a fuller understanding of the interaction between magnetic fields and convection in the laboratory, but in order to explain, for example, many of the observed characteristics in the solar photosphere and convection zone one must clearly look to the nonlinear problem which takes fully into account this interaction via the nonlinear coupling terms.

Early two-dimensional linear studies in hydromagnetic convection by Weiss (1966) were undertaken in the limit of a small magnetic field, with the investigation being restricted to the kinematic effects of the flow on the magnetic field, while the effect of the magnetic forces on the flow was neglected. Recently, Galloway and Proctor (1983) extended this kinematic study to a three-dimensional hexagonal geometry. The dynamic extension of the two-dimensional case has been thoroughly studied by Weiss (1981*a*, 1981*b*, 1981*c*). The nonlinear dynamical investigation of the hexagonal system presented in the present paper did not follow on from the earlier equivalent kinematic studies (e.g. Galloway and Proctor 1983), but rather developed from the modal approach for ordinary nonlinear Rayleigh–Benard convection.

0004-9506/85/010041$02.00

Another approach utilized has been to expand the variables in terms of their linear horizontal eigenfunctions, and then take horizontal averages. This method was pioneered by Roberts (1966) for ordinary Rayleigh–Benard convection, and has been extensively developed by other authors (Gough *et al.* 1975; Toomre *et al.* 1982; Murphy and Lopez 1984; Lopez and Murphy 1984). Authors employing this method in the past to study the magnetoconvection problem have chosen the eigenfunctions, which determine the cellular planforms, in such a way that the equations reduce to the so-called mean-field equations. An equivalent formulation may also be obtained from a Galerkin-type method (Van der Borght *et al.* 1972).

The modal method together with an appropriate choice of eigenfunction can also be used to model three-dimensional hexagonal cellular convection, which incorporates the effects of interactions between neighbouring cells. This approach has been adopted here to establish the global characteristics of convective heat transport in hexagonal cells under the effect of an imposed magnetic field. Proctor and Galloway (1979) have indicated that: 'It would also be most desirable to extend the theory of a hexagonal convective pattern so as to model the convection zone more closely, but this appears to require significant computational effort.' Galloway and Weiss (1981) further designated the need for three-dimensional solutions by presenting an argument suggesting that the two-dimensional flux sheet solutions should be unstable in the dynamic regime of the problem.

In another recent paper, Knobloch (1981) called for a magnetoconvective model which simulates the observed different scales of magnetic flux tubes arising as a result of the different scales of motion present in the Sun. The models which are presently available (Proctor and Galloway 1979; Weiss 1981*a*, 1981*b*, 1981*c*) do not provide an explanation of the observed spectrum. Galloway and Weiss (1981) also suggested the use of a two scale analysis—one associated with the cellular convection and the other with the small scale eddies representing turbulence. It is anticipated that the modal approach employed here can be extended to include many more scales of motion, so as to model the interactions observed between the different scales of motion (Golub *et al.* 1981; Knobloch and Rosner 1981). Multi-mode solutions using the modal approach have already been presented for the ordinary Rayleigh–Benard problem by Toomre *et al.* (1982).

It is well known, from the linear theory, that when the ratio of magnetic diffusivity η to thermal diffusivity κ is sufficiently small, or when the applied magnetic field is large enough, instabilities set in as oscillatory modes, giving rise to time-dependent solutions in the nonlinear regime. In this study we only set out to establish steady-state solutions, but at the same time provide a basis from which to solve and understand the more complicated time-dependent problem in future studies involving magnetic fields.

2. Basic Equations and Numerical Technique

The model problem investigated is the interaction between a uniform vertical magnetic field and a horizontal layer of fluid, between two isothermal stress-free boundaries, and which is heated from below. The equations describing the physical processes present are the momentum equation

$$\rho \frac{\partial \boldsymbol{u}}{\partial t} + \rho \boldsymbol{u} . \nabla \boldsymbol{u} + \nabla P - \rho \boldsymbol{G} - \mu \nabla^2 \boldsymbol{u} + \frac{\mu^*}{4\pi} \boldsymbol{H} \times (\nabla \times \boldsymbol{H}) = 0, \tag{1}$$

together with the continuity equation

$$\partial\rho/\partial t + \nabla.(\rho \boldsymbol{u}) = 0, \tag{2}$$

as well as the induction equation

$$\partial \boldsymbol{H}/\partial t + \eta\nabla \times (\nabla \times \boldsymbol{H}) - \nabla \times (\boldsymbol{u} \times \boldsymbol{H}) = 0, \tag{3}$$

and the heat equation

$$\rho C_V \partial T/\partial t + \rho C_v \boldsymbol{u}.\nabla T - K\nabla^2 T = 0, \tag{4}$$

where μ, K, C_V and μ^* are respectively the viscosity, the thermal conductivity, the specific heat at constant volume, and the magnetic permeability, and $\boldsymbol{G}$ is $(0, 0, g)$, g being the acceleration due to gravity. For the purposes of this study the Boussinesq approximation will be utilized, viscous dissipation effects neglected and only steady-state solutions considered.

The basic equations may be derived by following the procedure of Van der Borght and Murphy (1973), or alternatively by a Galerkin procedure similar to that used by Gough *et al.* (1975). After appropriate rescaling (Van der Borght and Murphy 1973), the basic equations may be written in their non-dimensional form:

$$\mathrm{D}^2 T_0 - \mathrm{D}(FW) = 0, \tag{5}$$

$$(\mathrm{D}^2 - a^2)F - W\mathrm{D}T_0 - C(2W\mathrm{D}F + F\mathrm{D}W) = 0, \tag{6}$$

$$\begin{aligned}(\mathrm{D}^2 - a^2)^2 W - Ra^2 F + Q\tau\mathrm{D}(\mathrm{D}^2 - a^2)H \\ -(C/\sigma)\{W(\mathrm{D}^2 - a^2)\mathrm{D}W + 2(\mathrm{D}^2 - a^2)W\mathrm{D}W + 3Z\mathrm{D}Z\} \\ + Q\tau C\{H(\mathrm{D}^2 - a^2)\mathrm{D}W + 2(\mathrm{D}^2 - a^2)H\mathrm{D}H + 3\chi\mathrm{D}\chi\} = 0,\end{aligned} \tag{7}$$

$$\begin{aligned}\tau(\mathrm{D}^2 - a^2)^2 H + \mathrm{D}(\mathrm{D}^2 - a^2)W \\ + C\{\mathrm{D}H\mathrm{D}^2 W - \mathrm{D}W\mathrm{D}^2 H + H(\mathrm{D}^2 - a^2)\mathrm{D}W - W(\mathrm{D}^2 - a^2)\mathrm{D}H\} = 0,\end{aligned} \tag{8}$$

$$\tau(\mathrm{D}^2 - a^2)\chi + \mathrm{D}Z - \mathrm{C}(2\chi\mathrm{D}W - 2Z\mathrm{D}H - H\mathrm{D}Z + W\mathrm{D}\chi) = 0, \tag{9}$$

$$(\mathrm{D}^2 - a^2)Z + Q\tau\mathrm{D}\chi - (C/\sigma)(W\mathrm{D}Z - Z\mathrm{D}W) - Q\tau C(\chi\mathrm{D}H - H\mathrm{D}\chi) = 0, \tag{10}$$

where $\mathrm{D} \equiv \mathrm{d}/\mathrm{d}z$.

The temperature, velocity, vorticity, magnetic field and current density are given by

$$T = T_0(z) + F(z)f, \tag{11}$$

$$\boldsymbol{u} = \left\{\frac{1}{a^2}\left(\mathrm{D}W(z)\frac{\partial f}{\partial x} + Z(z)\frac{\partial f}{\partial y}\right), \frac{1}{a^2}\left(\mathrm{D}W(z)\frac{\partial f}{\partial y} - Z(z)\frac{\partial f}{\partial x}\right), W(z)f\right\}, \tag{12}$$

$$\boldsymbol{\omega} = \left\{\frac{1}{a^2}\left(\mathrm{D}Z(z)\frac{\partial f}{\partial x} - (\mathrm{D}^2 - a^2)W(z)\frac{\partial f}{\partial y}\right),\ \frac{1}{a^2}\left(\mathrm{D}Z(z)\frac{\partial f}{\partial y} + (\mathrm{D}^2 - a^2)W(z)\frac{\partial f}{\partial x}\right),\ Z(z)f\right\}, \tag{13}$$

$$\boldsymbol{H} = H_0\left\{\frac{1}{a^2}\left(\mathrm{D}H(z)\frac{\partial f}{\partial x} + \chi(z)\frac{\partial f}{\partial y}\right),\right.$$
$$\left.\frac{1}{a^2}\left(\mathrm{D}H(z)\frac{\partial f}{\partial y} - \chi(z)\frac{\partial f}{\partial x}\right),\ 1 + H(z)f\right\}, \tag{14}$$

$$\boldsymbol{\xi} = H_0\left\{\frac{1}{a^2}\left(\mathrm{D}\chi(z)\frac{\partial f}{\partial x} - (\mathrm{D}^2 - a^2)H(z)\frac{\partial f}{\partial y}\right),\right.$$
$$\left.\frac{1}{a^2}\left(\mathrm{D}\chi(z)\frac{\partial f}{\partial y} + (\mathrm{D}^2 - a^2)H(z)\frac{\partial f}{\partial x}\right),\ \chi(z)f\right\}, \tag{15}$$

Z and χ being the scaled vertical components of vorticity and current density, while W, F and H define the vertical velocity, the temperature fluctuation and the induced vertical magnetic field; T_0 is the mean temperature across the layer and H_0 the strength of the externally applied vertical magnetic field. The temperature difference across the layer is denoted by ΔT and a is the horizontal wave number, while f is the planform function which satisfies the Helmholtz equation

$$\partial^2 f(x,y)/\partial x^2 + \partial^2 f(x,y)/\partial y^2 = -a^2 f(x,y), \tag{16}$$

and C, the interaction constant, takes the value of $\sqrt{\frac{1}{6}}$ in the case where

$$f(x,y) = (\tfrac{2}{3})^{\frac{1}{2}}\{2\cos(\tfrac{1}{2}a\sqrt{3}\,x)\cos(\tfrac{1}{2}ay) + \cos(ay)\}$$

describes a hexagonal planform. If $C = 0$, then the basic equations reduce to the mean-field equations.

The other parameters in the basic equations are the Rayleigh number $R = g\alpha d^3\Delta T/\kappa\nu$ (d being the depth of the layer, α the coefficient of volume expansion and ν the viscous diffusivity), the Chandrasekhar number $Q = \mu^* d^2 H_0^2/4\pi\mu\eta$, the Prandtl number $\sigma = \nu/\kappa$, and the magnetic Prandtl number $\tau = \eta/\kappa$.

Equation (5) has a first integral in which the constant of integration is the Nusselt number

$$N = FW - \mathrm{D}T_0. \tag{17}$$

The Nusselt number is the ratio of heat transported by the convective regime to that which would have been transported if the fluid were immobilized, thus defining a non-dimensional heat flux.

Equations (5)–(10) have been solved together with the free-surface boundary conditions, which are widely used in stellar applications. The boundaries are taken to be isothermal, with

$$F(z=0) = F(z=1) = 0, \tag{18}$$

$$T_0(z=0) = 0, \qquad T_0(z=1) = -1. \tag{19}$$

Also, there is no overshooting at the boundaries, and no tangential stresses on them; hence

$$W = \mathrm{D}^2 W = \mathrm{D}Z = 0 \tag{20}$$

on $z = 0$ and $z = 1$, and the boundaries are taken to be non-conducting and current-free, implying that

$$\mathrm{D}H = \chi = 0 \tag{21}$$

on $z = 0$ and $z = 1$.

Due to the highly nonlinear nature of the equations, numerical solutions are necessary. A collocation procedure was employed using truncated Fourier expansions, an approach which has been successfully used in a number of convection problems (Roberts 1966; Murphy 1971; Van der Borght *et al.* 1972; Van der Borght and Murphy 1973; Van der Borght *et al.* 1974; Murphy and Lopez 1984; Lopez and Murphy 1984).

The variables are expanded in the following manner (where M is the number of vertical modes):

$$W(z) = \sum_{n=1}^{M} W_n \sin(n\pi z), \qquad F(z) = \sum_{n=1}^{M} f_n \sin(n\pi z), \tag{22a, b}$$

$$T_0(z) = -z + \sum_{n=1}^{M} t_n \sin(n\pi z), \qquad H(z) = h_0 + \sum_{n=1}^{M} h_n \cos(n\pi z), \tag{22c,d}$$

$$\chi(z) = \sum_{n=1}^{M} \chi_n \sin(n\pi z), \qquad Z(z) = L_0 + \sum_{n=1}^{M} L_n \cos(n\pi z), \tag{22e, f}$$

which clearly satisfy the boundary conditions adopted.

Substitution of the above Fourier expansions into equations (5)–(10), where the notation

$$R_1 = R/\pi^4, \quad \omega_n = W_n/\pi^4, \quad \alpha^2 = a^2/\pi^2, \quad Y(n) = \begin{cases} 1, & n > 0 \\ 0, & n = 0 \\ -1, & n < 0 \end{cases} \tag{23}$$

has been used, gives the following system of nonlinear algebraic equations for the unknown coefficients in these expansions:

$$(n^2+\alpha^2)^2\omega_n - R_1\alpha^2 f_n + \frac{Q\tau}{\pi^3} n(n^2+\alpha^2)h_n + \frac{CQ\tau}{\pi^3} n(n^2+3\alpha^2)h_0 h_n$$

$$+ \frac{C\pi}{2\sigma} \sum_p \omega_p \{|n-p|(3\alpha^2+3p^2+n^2-2np)\omega_{|n-p|}$$

$$-(n+p)(3\alpha^2+3p^2+n^2+2np)\omega_{n+p}\}$$

$$+ \frac{CQ\tau}{2\pi^3} \sum_p h_p p\{(3p^2+3\alpha^2+2n^2-4np)h_{|n-p|} - (3\alpha^2+3p^2+2n^2+4np)h_{n+p}\}$$

$$+ \frac{3C}{2\sigma\pi^5} \sum_p L_p\{(n+p)L_{n+p} + (n-p)L_{|n-p|}\} + \frac{3C}{\sigma\pi^5} nL_0 L_n$$

$$+\frac{3CQ\tau}{2\pi^5}\sum_p \chi_p\{|n-p|\chi_{|n-p|}-(n+p)\chi_{n+p}\} = 0, \tag{24}$$

$$nt_n - \tfrac{1}{2}\pi\sum_p \omega_p\{f_{n+p}+Y(p-n)f_{|n-p|}\} = 0, \tag{25}$$

$$(n^2+\alpha^2)f_n-\omega_n-\tfrac{1}{2}\pi\sum_p \omega_p\{(n+p)t_{n+p}-|n-p|t_{|n-p|}\}$$

$$-\tfrac{1}{2}C\pi\sum_p \omega_p\{(2n+p)f_{n+p}+Y(n-p)(p-2n)f_{|n-p|}\} = 0, \tag{26}$$

$$(n^2+\alpha^2)h_n - \frac{n\pi}{\tau}\omega_n - \frac{Cn\pi}{\tau}h_0\omega_n$$

$$-\frac{C\pi}{2\tau}\sum_p \omega_p\{(2p+n)h_{n+p}+(2p-n)h_{|n-p|}\} = 0, \tag{27}$$

$$\alpha^2 h_0 - \frac{C\pi}{\tau}\sum_p p\omega_p h_p = 0, \tag{28}$$

$$(n^2+\alpha^2)L_n - \frac{Q\tau}{\pi}n\chi_n - \frac{C\pi}{\sigma}nL_0\omega_n - \frac{CQ\tau}{\pi}nh_0\chi_n$$

$$-\frac{C\pi}{2\sigma}\sum_p \omega_p\{(2p+n)L_{n+p}+(2p-n)L_{|n-p|}\}$$

$$-\frac{CQ\tau}{2\pi}\sum_p \chi_p\{(2p+n)h_{n+p}+(2p-n)h_{|n-p|}\} = 0, \tag{29}$$

$$\alpha^2 L_0 - \frac{C\pi}{\sigma}\sum_p pL_p\omega_p - \frac{CQ\tau}{\pi}\sum_p p\chi_p h_p = 0, \tag{30}$$

$$(n^2+\alpha^2)\chi_n + \frac{nL_n}{\pi\tau} + \frac{2C}{\pi\tau}nL_0 h_n + \frac{C}{\pi\tau}nh_0 L_n$$

$$+\frac{C\pi}{2\tau}\sum_p \omega_p\{(p-n)\chi_{n+p}+Y(n-p)(n+p)\chi_{|n-p|}\}$$

$$+\frac{C}{2\pi\tau}\sum_p h_p\{(n-p)L_{n+p}+(n+p)L_{|n-p|}\} = 0. \tag{31}$$

The system of equations (24)–(31) was solved on an iterative basis by using the generalized Newton–Raphson procedure. The number of vertical modes M is chosen so that in any particular solution the Nusselt number remains constant over the entire layer. In physical terms, this means that enough modes have to be included to properly resolve the boundary layers numerically.

Employing the Newton–Raphson technique requires the first derivatives of these equations, and the problem reduces to that of solving a $(6M+2)\times(6M+3)$ augmented matrix at each iteration. For $R = 10^5$, at least 80 vertical modes were required to

obtain the necessary resolution, which clearly gives a very large system of equations to be solved.

3. Results

In an earlier study of the non-magnetic case (Murphy and Lopez 1984), it was found that two distinct types of solutions exist in certain parameter ranges and are distinguished by their components of vertical vorticity. For one type the vertical vorticity is zero, whereas for the other it is nonzero, and consequently significant features of the flow differ between the two solutions. Here we have restricted our study to a close examination of the steady-state solutions which possess zero components of vertical vorticity and current density in order to establish the effects of a hexagonal geometry and the influences of the Prandtl and magnetic Prandtl numbers. There is, however, an apparently strong association between the nonzero vertical component of vorticity and time-dependent behaviour (Lopez and Murphy 1983), and presumably the vertical component of current density is also related.

The system is now determined by six parameters: the Rayleigh number R and the Chandrasekhar number Q which describe the external influences acting on the system, the Prandtl and magnetic Prandtl numbers σ and τ which describe physical characteristics of the fluid, and finally a and C which describe the geometry of the flow. A complete scan of the available parameter space is quite impractical, hence certain parameters will remain fixed, while others, which are felt to demonstrate a significant varying behaviour of the convective solutions under the presence of a magnetic field, are scanned thoroughly. The geometry of the flow is described throughout by a hexagonal cell pattern, for which $C = \sqrt{\frac{1}{6}}$ with a non-dimensional horizontal wave number $a = 2{\cdot}63$. Two values of the Rayleigh number have been investigated, a moderate value of 3×10^4 and a larger value of 3×10^5. The highest value of the Rayleigh number utilized in two-dimensional nonlinear magneto-convection results, published to date, is 10^5 (Weiss 1981*c*). The Chandrasekhar number has been varied from 1 to 10^4, while the Prandtl and magnetic Prandtl numbers have both been extensively varied within the range 10^{-2}–10^3.

The flow and magnetic field structures in this three-dimensional hexagonal system are quite different from those found in two-dimensional studies. The concepts of two-dimensional flux sheets and flux expulsion do not relate directly to our present system. Typically, what has been found is that a perturbed magnetic field is induced at the bottom of the layer and concentrated around the centre of the cell base, which is a region of convergent flow. Further, near the top of the vertical boundaries of the cell, as the field is swept around, there is considerable field dispersion in these regions of divergent flow—a manifestation of the tendency of the magnetic field lines to align with the streamlines of the flow. This behaviour is reminiscent of the solar situation, where it is expected that the magnetic field is generated and anchored at the base of the convective zone (the effects of differential rotation tend to support this idea), and where intense magnetic fields are seen to be concentrated at the boundaries of supergranules (Priest 1982).

From our selection of parameter values, extensive numerical results have been obtained which present a global picture of three-dimensional flow inside hexagonal cells. The following discussion is a description of the flow characteristics as the magnetic Prandtl number τ is varied, with $R = 3 \times 10^5$, $\sigma = 1$ and $Q = 100$. These features are graphically shown in Figs 1*a–c* where the velocity (top) and magnetic

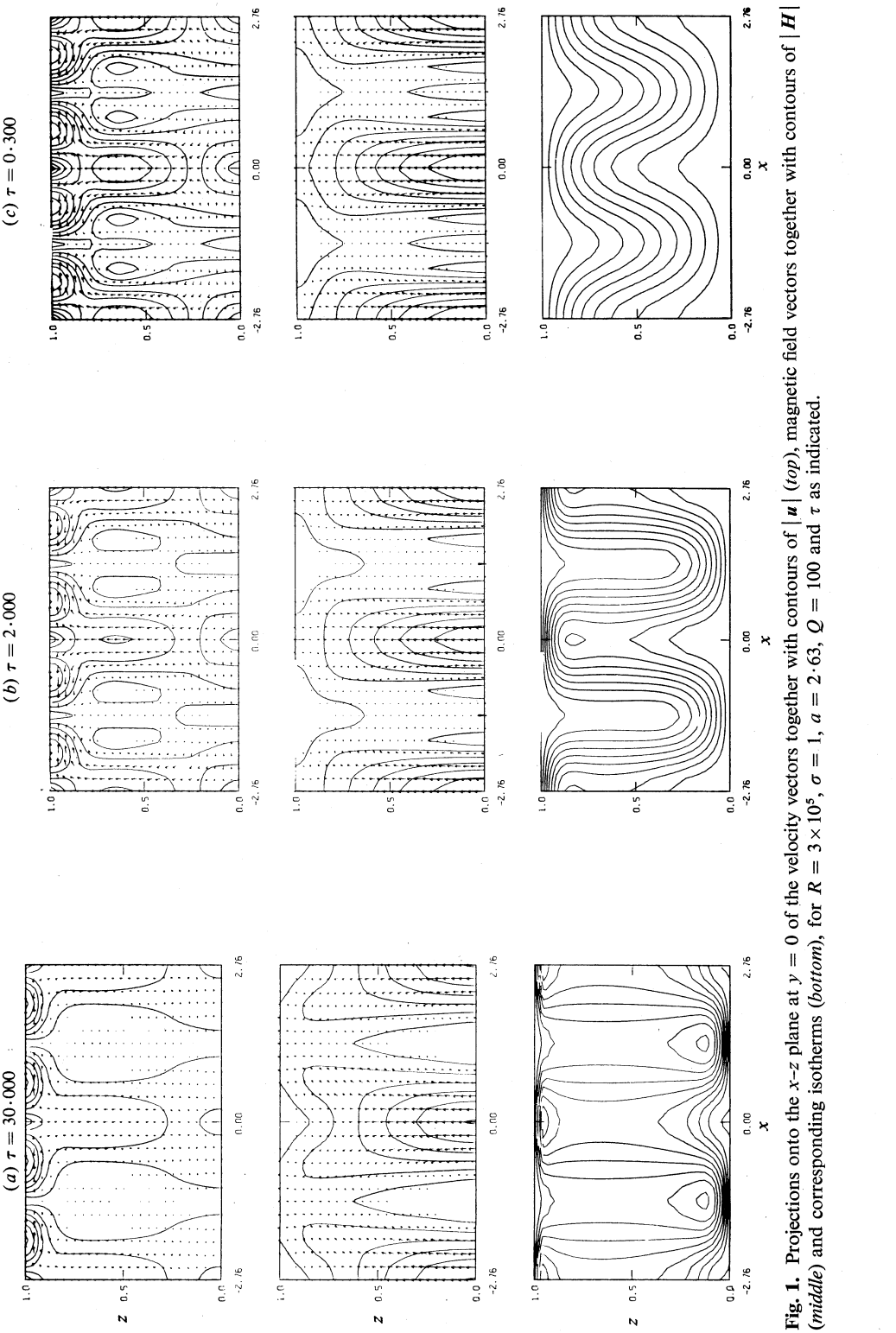

Fig. 1. Projections onto the x–z plane at $y = 0$ of the velocity vectors together with contours of $|\boldsymbol{u}|$ (*top*), magnetic field vectors together with contours of $|\boldsymbol{H}|$ (*middle*) and corresponding isotherms (*bottom*), for $R = 3 \times 10^5$, $\sigma = 1$, $a = 2{\cdot}63$, $Q = 100$ and τ as indicated.

field (middle) vectors are projected onto the x–z plane at $y = 0$, together with contours of their strength, as well as plots of the isotherms (bottom).

At large τ (Fig. 1*a*), the flow is essentially restricted to the top 10% of the layer, while the field, as shown by the contours of field strength, is concentrated at the bottom centre of the cells in spite of the relatively low fluid velocity in this region. Clearly, stronger fields are induced in regions of convergent fluid flow within the hexagonal cell, and there is a weak or no perturbed field generated in regions of divergent flow. An investigation of the isotherms reveals the existence of extensive isothermal regions in the central part of the layer with rapid temperature changes occurring near both the top and bottom of the cell, that at the top being much more pronounced.

As τ is reduced, the convective flow, although its speed is considerably reduced, extends more uniformly throughout the layer (see Fig. 1*c*) but is still not symmetric about the mid-plane $z = 0{\cdot}5$. The structure of the magnetic field is such that it is more concentrated towards the centre of the cell with the isotherms designating a smoothing of the temperature variations across the layer.

The flow characteristics also vary dramatically as the Prandtl number σ is varied. This is illustrated in Figs 2*a–f* where $R = 3 \times 10^4$, $\tau = 10$ and $Q = 10$. At low σ (Figs 2*a* and 2*b*), the fluid is nearly stagnant over most of the layer, except for about the top 5–10% where there is relatively vigorous boundary layer activity. The associated field is essentially uniform throughout the layer, with the induced field being virtually non-existent. The isotherms display the monotonic nature of the mean temperature.

As σ increases, the boundary layer is relaxed as the flow now extends deeper into the layer, with the stagnant regions being restricted to the vertical boundaries of the cells (see Figs 2*c* and 2*d*). The magnetic field is now swept with the fluid to a greater extent so that it is concentrated into regions of convergent fluid flow. Fig. 2*f* shows that at the bottom of the layer it is concentrated in the central cell region, and at the top, towards the vertical cell boundaries. The isotherms show the development of hot plumes rising in the centre and cold plumes descending at the boundaries of the cells.

As σ becomes larger, a field interaction between neighbouring cells is evident near the vertical boundaries at the top of the layer, as the field is swept horizontally because of the high fluid velocities. Reduced field strength at the centre of the cell at the top of the layer again corresponds to regions of divergent flow. When $\sigma = 100$ (Fig. 2*f*), the fluid flow is very nearly symmetric about the middle of the layer $z = 0{\cdot}5$, as established for the mean-field situation, yet the magnetic field structure is completely different to that corresponding to the mean-field solutions (cf. Van der Borght *et al.* 1972). Whereas in the mean-field model the magnetic field is symmetric about the mid-plane $z = 0{\cdot}5$, with most of the field concentrated near the top and bottom of the layer, the field in the hexagonal situation is concentrated deep at the base of the cell and is swept around considerably in the upper part of the layer causing diminished strength.

Figs 3 and 4 summarize three basic regions in τ space with different types of behaviour:

(i) For large τ ($\gtrsim 10^2$), N is found to be constant with respect to τ and behaves as previously determined in the mean-field case with respect to Q. The induced field is smaller as τ increases and is independent of Q, when Q is not too large.

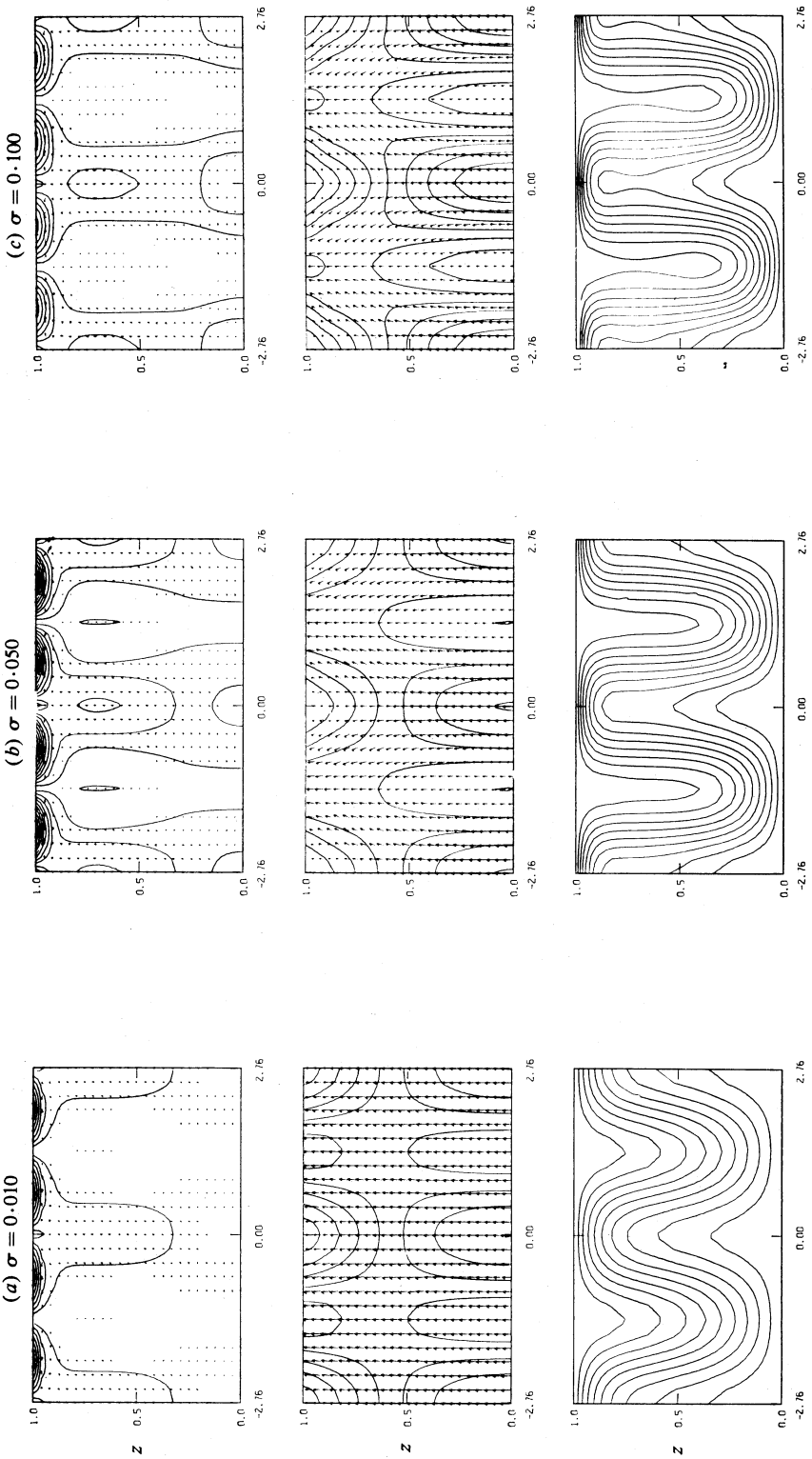

Figs 2a–2c.

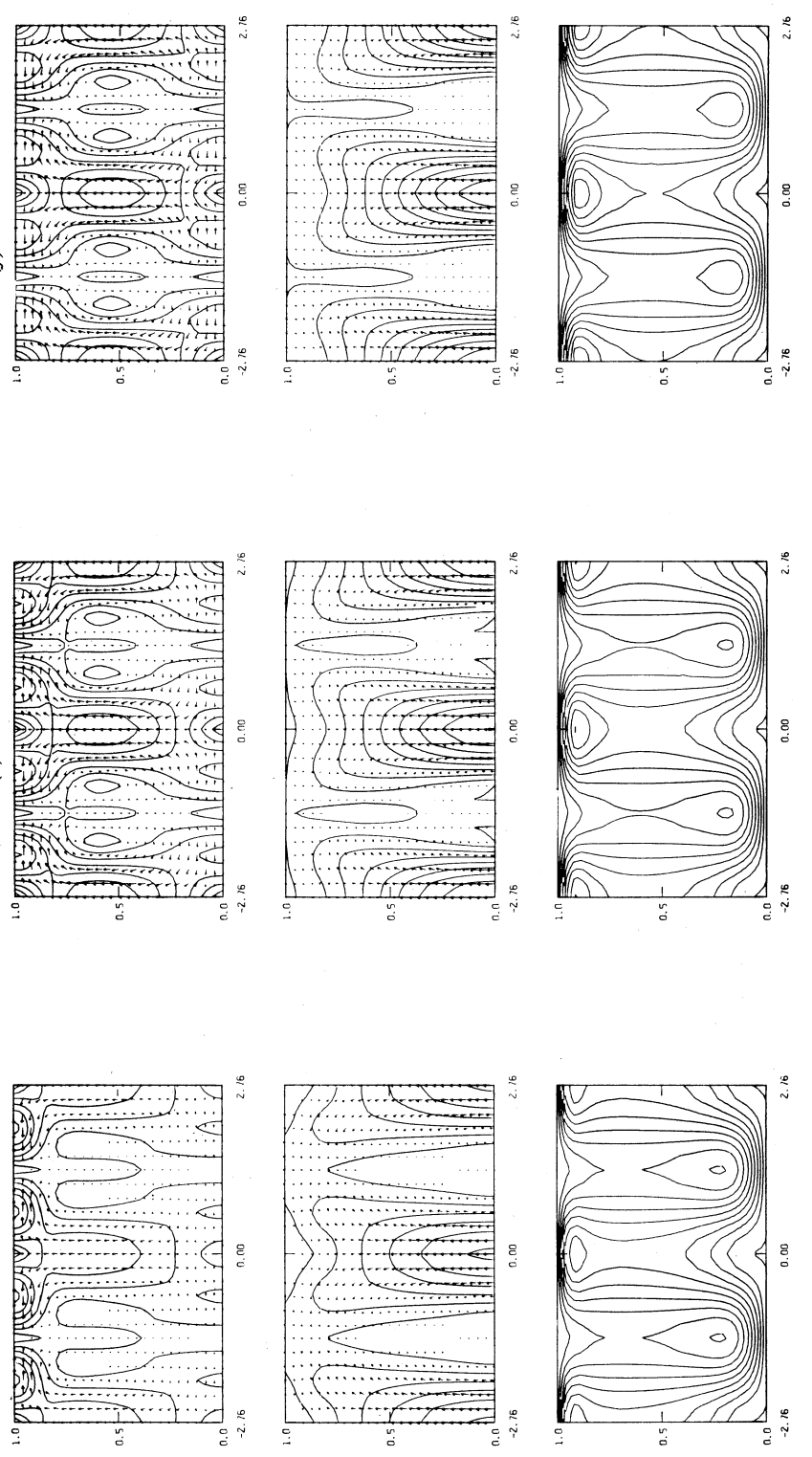

Fig. 2. Projections onto the x–z plane at $y = 0$ of the velocity vectors together with contours of $|\boldsymbol{u}|$ (*top*), magnetic field vectors together with contours of $|\boldsymbol{H}|$ (*middle*) and corresponding isotherms (*bottom*), for $R = 3 \times 10^4$, $a = 2{\cdot}63$, $Q = 10$, $\tau = 10$ and σ as indicated.

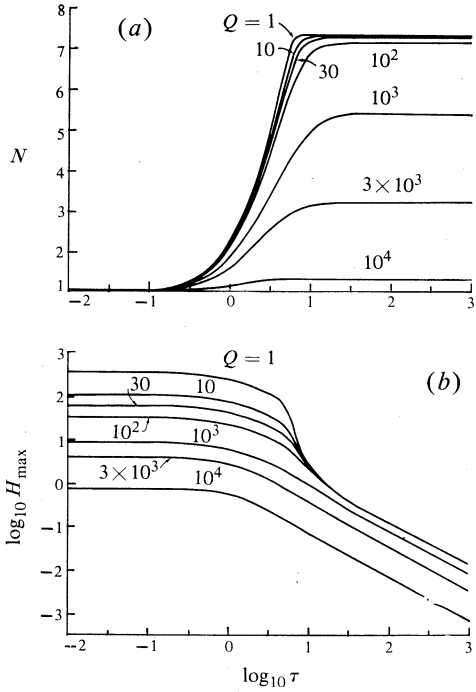

Fig. 3. Variation with τ of (*a*) Nusselt number N and (*b*) maximum vertical induced magnetic field H_{max}, for $R = 3\times10^5$, $\sigma = 0{\cdot}1$, $a = 2{\cdot}63$ and Q as indicated.

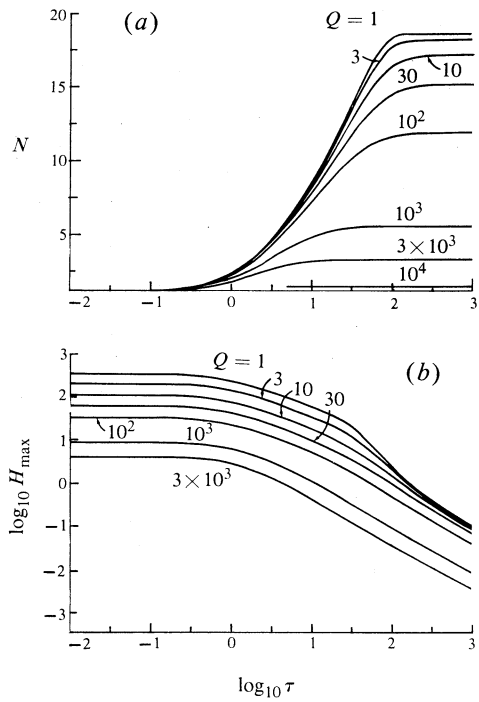

Fig. 4. Variation with τ of (*a*) Nusselt number N and (*b*) maximum vertical induced magnetic field H_{max}, for $R = 3\times10^5$, $\sigma = 100$, $a = 2{\cdot}63$ and Q as indicated.

(ii) For intermediate τ ($10^{-1} \lesssim \tau \lesssim 10^{2}$) there is a very marked variation in N over a small region of τ. This demonstrates the existence of a critical balance between the diffusivities, which determines whether a magnetic field is to inhibit convection or not. In this range of τ, we find that the extent to which the field is induced depends strongly on Q. Overall the smaller the value of Q, the greater the induced field relative to the impressed field.

(iii) For small τ ($\lesssim 10^{-2}$) the Nusselt number now tends towards one, irrespective of σ, R or Q, so that any convective motions have been almost completely inhibited by the field, and $H_{\max}$ tends towards an upper limit as τ tends to zero. In particular, these results establish, for the range of Rayleigh numbers considered here, that the effect of σ on these regions appears to be only quantitative.

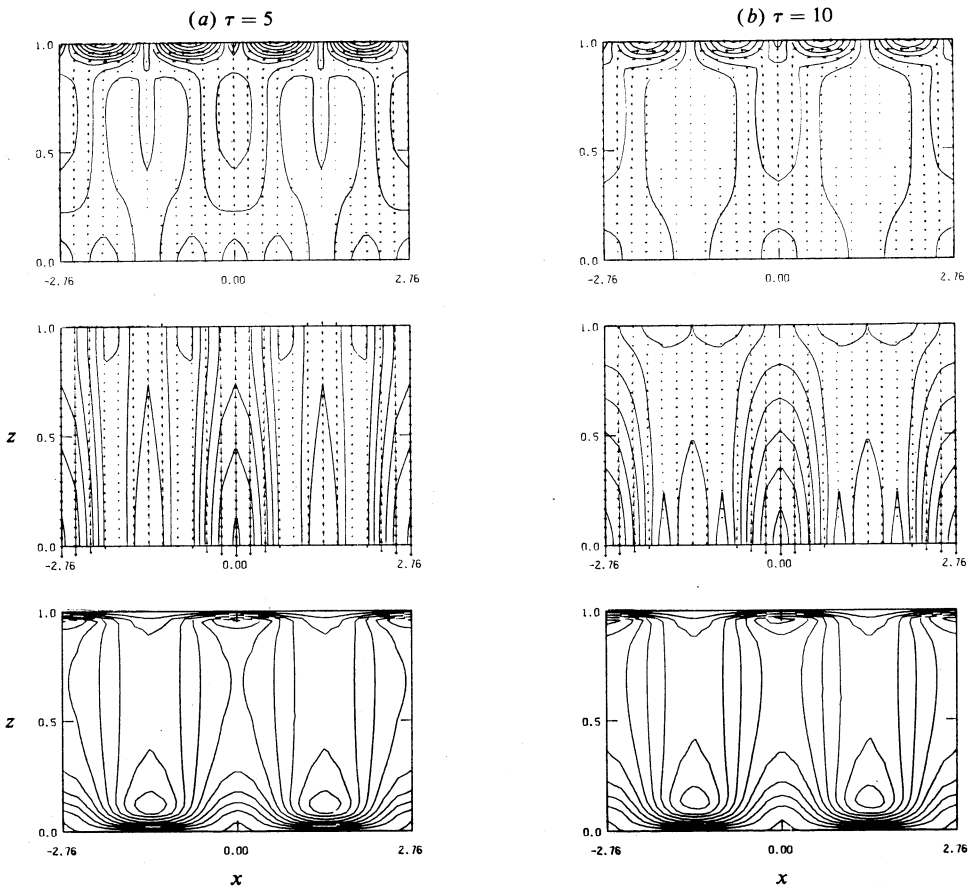

Fig. 5. Projections onto the x–z plane at $y = 0$ of the velocity vectors together with contours of $|\boldsymbol{u}|$ (*top*), magnetic field vectors with contours of $|\boldsymbol{H}|$ (*middle*), and corresponding isotherms (*bottom*) for $R = 3\times10^{5}$, $\sigma = 1$, $a = 2{\cdot}63$, $Q = 10$ and τ as indicated.

In the τ regions classified in (i) and (ii), two new types of solutions were found. It is felt that even though these are mathematically valid solutions of the system of equations in both cases, they do not, however, represent the model as the results are physically unacceptable. The non-physical properties of the two new solutions are

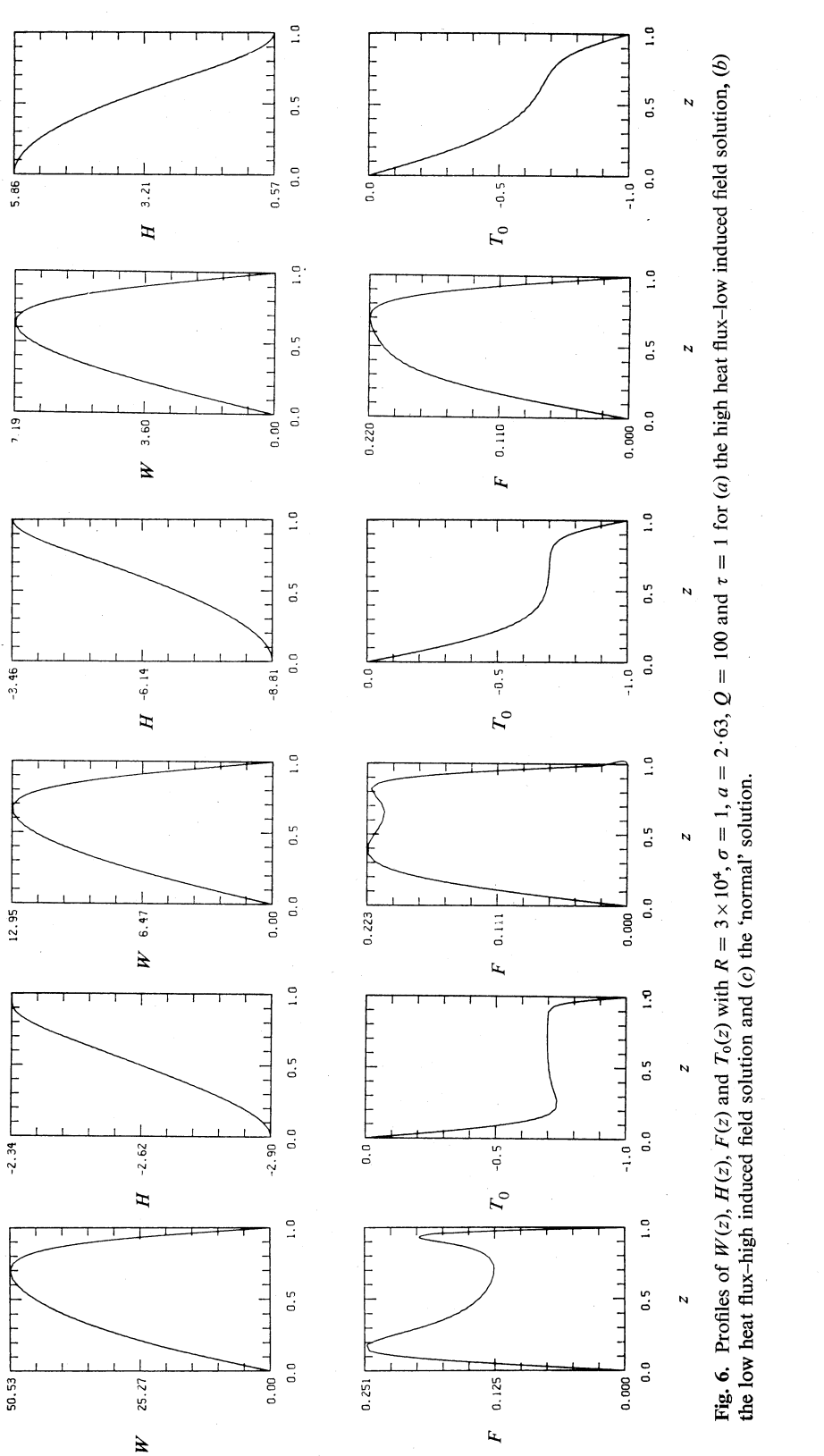

Fig. 6. Profiles of $W(z)$, $H(z)$, $F(z)$ and $T_0(z)$ with $R = 3\times10^4$, $\sigma = 1$, $a = 2{\cdot}63$, $Q = 100$ and $\tau = 1$ for (*a*) the high heat flux–low induced field solution, (*b*) the low heat flux–high induced field solution and (*c*) the 'normal' solution.

evident from the vector field projections in Figs 5*a* and 5*b* which show that at the bottom boundary, the field is directed downwards whereas just outside the layer the uniform applied field is directed upwards, hence presenting a discontinuity at the boundary.

Sample profiles of two of the new solutions, together with that of a 'normal' physical solution for the same parameter values, have been plotted in Figs 6*a–c*. The most striking feature of these is that for the two new solutions H is negative, whereas for the normal solution it is always positive. It should be pointed out that these three solutions are not related by any symmetry relationships, such as

$$W(z) \to -W(1-z), \qquad H(z) \to H(1-z), \qquad F(z) \to -F(1-z),$$
$$T_0(z) \to -1-T_0(1-z), \qquad Z(z) \to -Z(1-z), \qquad \chi(z) \to \chi(1-z),$$

which exist for the system of equations (5)–(10); nor are they the magnetic equivalent of the type II solutions found in other convection studies (see e.g. Murphy and Lopez 1984).

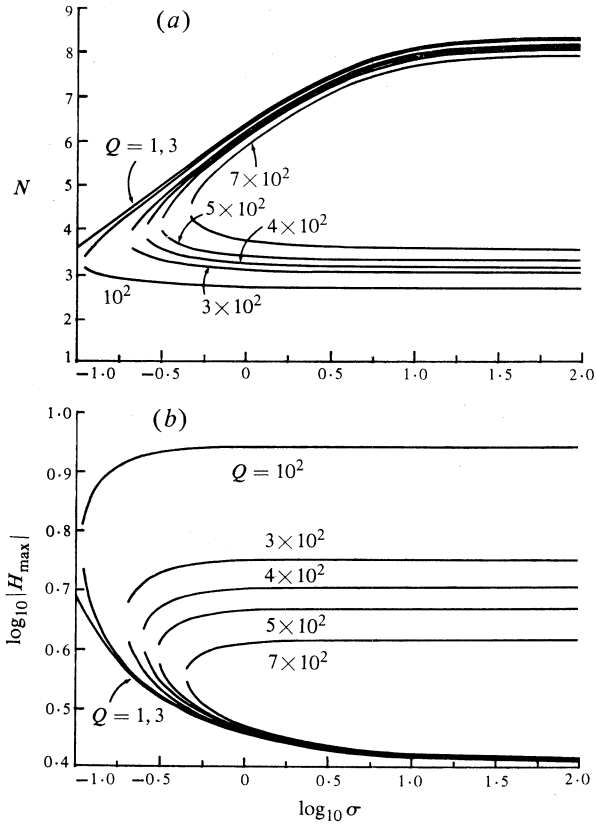

Fig. 7. Variation with σ of (*a*) Nusselt number N and (*b*) maximum vertical induced magnetic field $|H_{max}|$, for the high heat flux–low induced field solutions [upper branch in (*a*), lower branch in (*b*)] and the low heat flux–high induced field solutions [lower branch in (*a*), upper branch in (*b*)], for $R = 3\times10^4$, $\tau = 1$, $a = 2{\cdot}63$ and Q as indicated.

On comparison, the two new solutions have very distinctive differences. One specifically corresponds to a high heat flux–low induced field, and the other to a low heat flux–high induced field, with the two solutions tending to coalesce at low Prandtl number as shown in Fig. 7. The numerical method employed was unable to isolate the point at which the two coincide. As this point is approached the

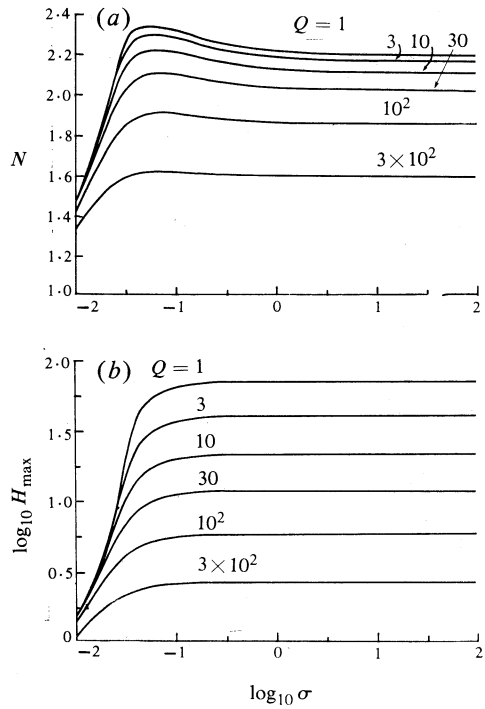

Fig. 8. Variation with σ of (*a*) Nusselt number N and (*b*) maximum vertical induced magnetic field $H_{\max}$, for $R = 3\times10^4$, $\tau = 1$, $a = 2{\cdot}63$ and Q as indicated.

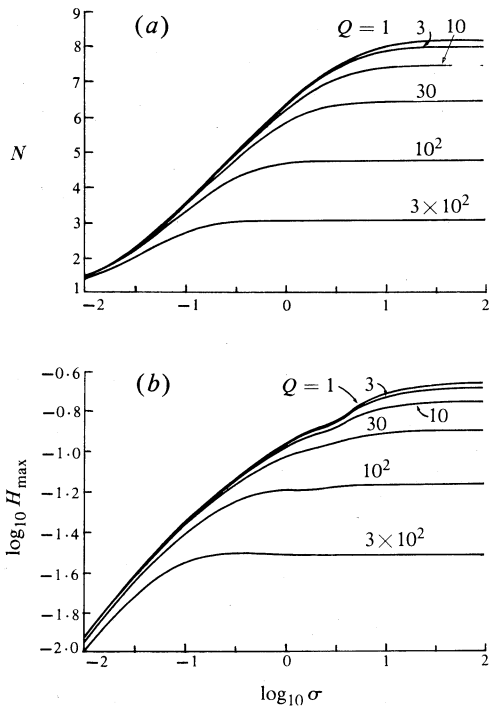

Fig. 9. Variation with σ of (*a*) Nusselt number N and (*b*) maximum vertical induced magnetic field $H_{\max}$, for $R = 3\times10^4$, $\tau = 100$, $a = 2{\cdot}63$ and Q as indicated.

difference between the two solutions is so small that the numerical system oscillated between the two, never converging onto one or the other.

The low heat flux solutions have a particularly non-physical feature in that N increases with Q, which is certainly not a dependence predicted by kinematic models, nor the mean-field model (Van der Borght *et al.* 1972).

The N–$\log\sigma$ curves of the 'normal' solutions for low Q, given in Fig. 8*a*, fit underneath those of the low heat flux branch of the alternative solutions from Fig. 7*a*. Whenever the 'non-physical' solutions exist mathematically, the 'normal' solutions corresponding to the same parameter set always have a lower Nusselt number, which means that the 'normal' solutions present a less efficient means of convective heat transport. This evident non-uniqueness of steady-state solutions can possibly be removed by considering the time-dependent solutions.

Unlike the non-magnetic case and the mean-field magnetic case, the normal N–$\log\sigma$ relationship is no longer always monotonic. The local maximum, which is evident in Fig. 8*a*, develops at lower σ as τ is reduced (cf. Fig. 9*a*), and is most pronounced at low τ and low Q. As σ tends to infinity, the system becomes independent of σ as is the case when $Q = 0$; and when σ tends to zero, the system tends towards the conductive state with no induced field.

In Figs 10 and 11, the profiles of $W(z)$, $H(z)$, $F(z)$ and $T_0(z)$ are illustrated varying with $\log\tau$ for $R = 3\times10^5$, $Q = 10^2$, $\sigma = 1$ and $a = 2{\cdot}63$, and also with $\log\sigma$ for $R = 3\times10^4$, $Q = 10$, $\tau = 10$ and $a = 2{\cdot}63$. The $W(z)$ profile, as τ is decreased below a critical τ value of ~10, decreases rapidly to zero in a monotonic fashion, whereas, when σ is decreased, the $W(z)$ profile reaches a local maximum at $\sigma \sim 1$ before it begins to decrease. The $F(z)$ and $T_0(z)$ profiles tend to behave similarly for both a decrease in σ and a decrease in τ. The main difference is that at low τ, the profile of $F(z)$ has almost completely vanished and the $T_0(z)$ profile reaches its linear configuration denoting a conductive state (Figs 10*c* and 10*d*), whereas from Figs 11*c* and 11*d*, the $F(z)$ profile has the two maxima at high σ, which denote the existence of thermal boundary layers, coalescing to one maximum giving the profile a fundamental sinusoidal mode at low σ, and the $T_0(z)$ profile displays small deviations from a linear profile when σ is reduced, which are effects typical of mild convection.

The variations of prime interest in this study are those of $H(z)$. As σ is lowered, the whole system tends closer to the conductive state, but does not reach it. However, as τ is decreased, all the variables tend towards their configuration at the conductive state except for $H(z)$ which grows quite markedly. This demonstrates the extent to which magnetic fields are amplified, and at the same time inhibit convective motions when the magnetic Prandtl number of the fluid is small. It should also be noted that at all times, the $H(z)$ profile shows that the bulk of the perturbed magnetic field is induced at the bottom boundary; this lends support to the conjecture that magnetic fields are generated and anchored at the base of convective envelopes (Priest 1982).

4. Concluding Remarks

The dynamic studies of steady hexagonal magnetoconvection, in a broad sense, agree with both the mean-field model (Van der Borght *et al.* 1972) and the kinematic model (Galloway and Proctor 1983). However, relationships which were monotonic in the previous cases are no longer so; this is attributed to the fact that the

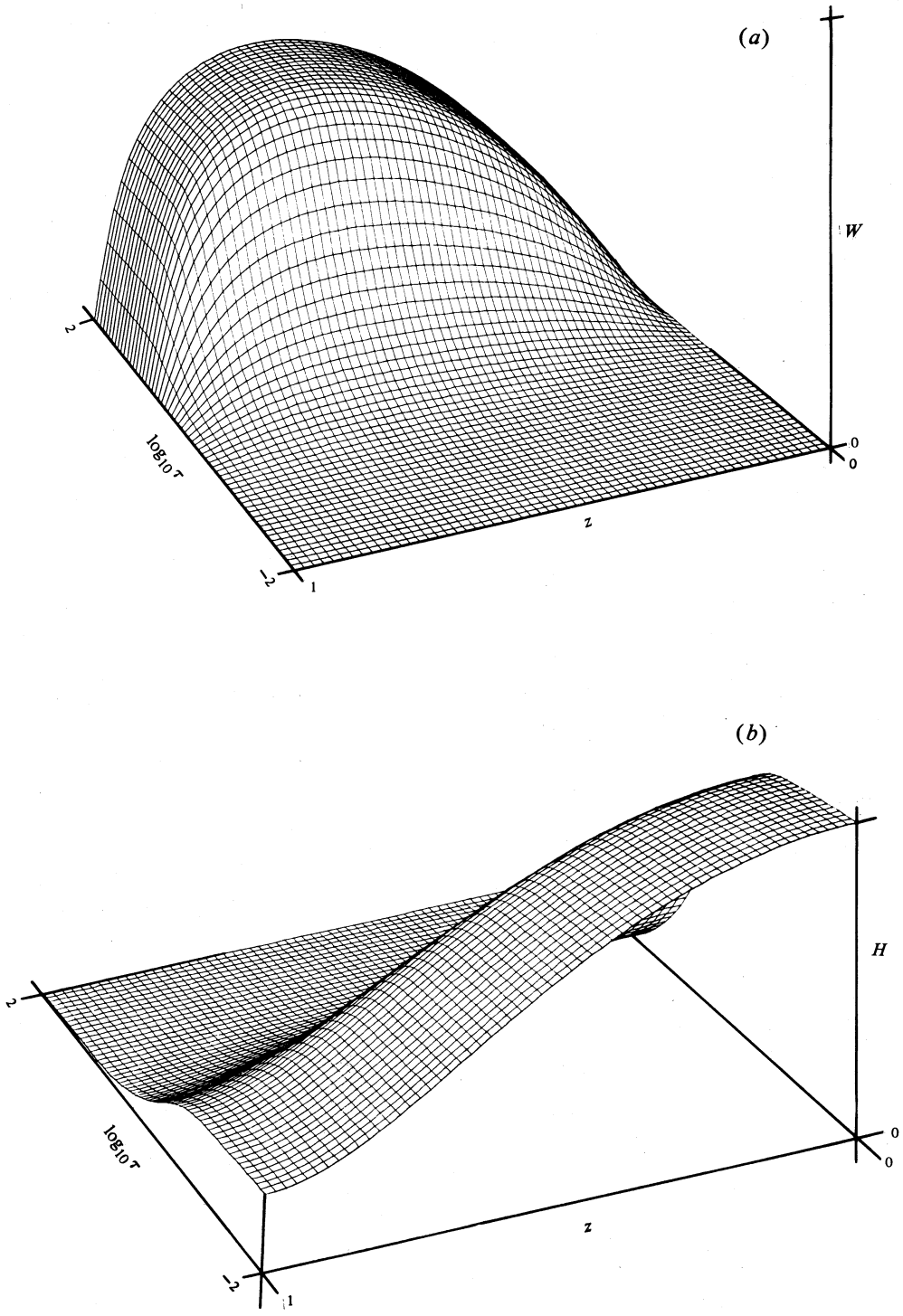

Fig. 10. Profiles over $0 \leqslant z \leqslant 1$ showing the variation with τ of the (*a*) vertical velocity $W(z)$, (*b*) induced vertical magnetic field $H(z)$, (*c*) temperature fluctuation $F(z)$ and (*d*) mean temperature $T_0(z)$, for $R = 3 \times 10^5$, $Q = 100$, $\sigma = 1$ and $a = 2{\cdot}63$.

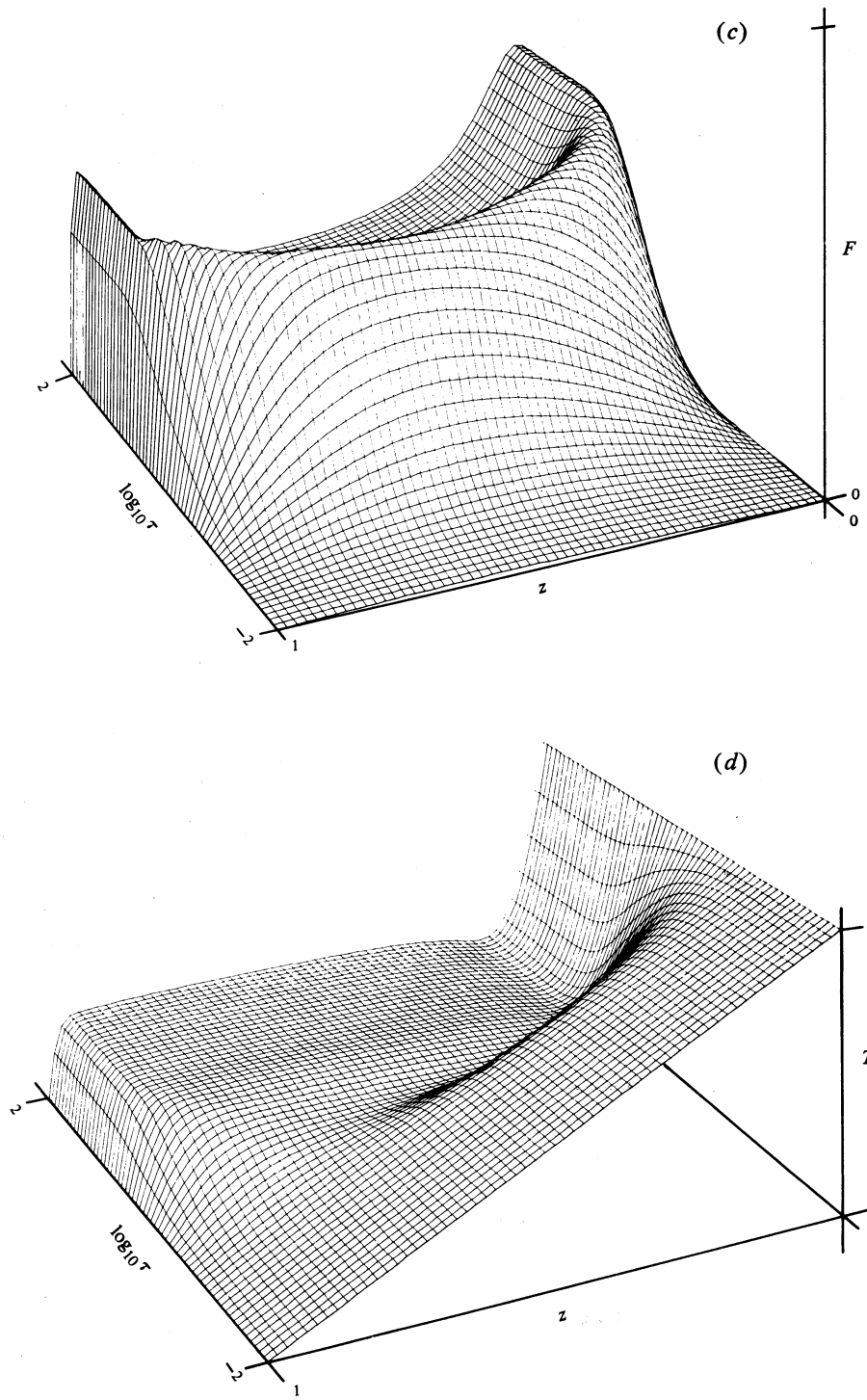

Figs 10*c* and 10*d*.

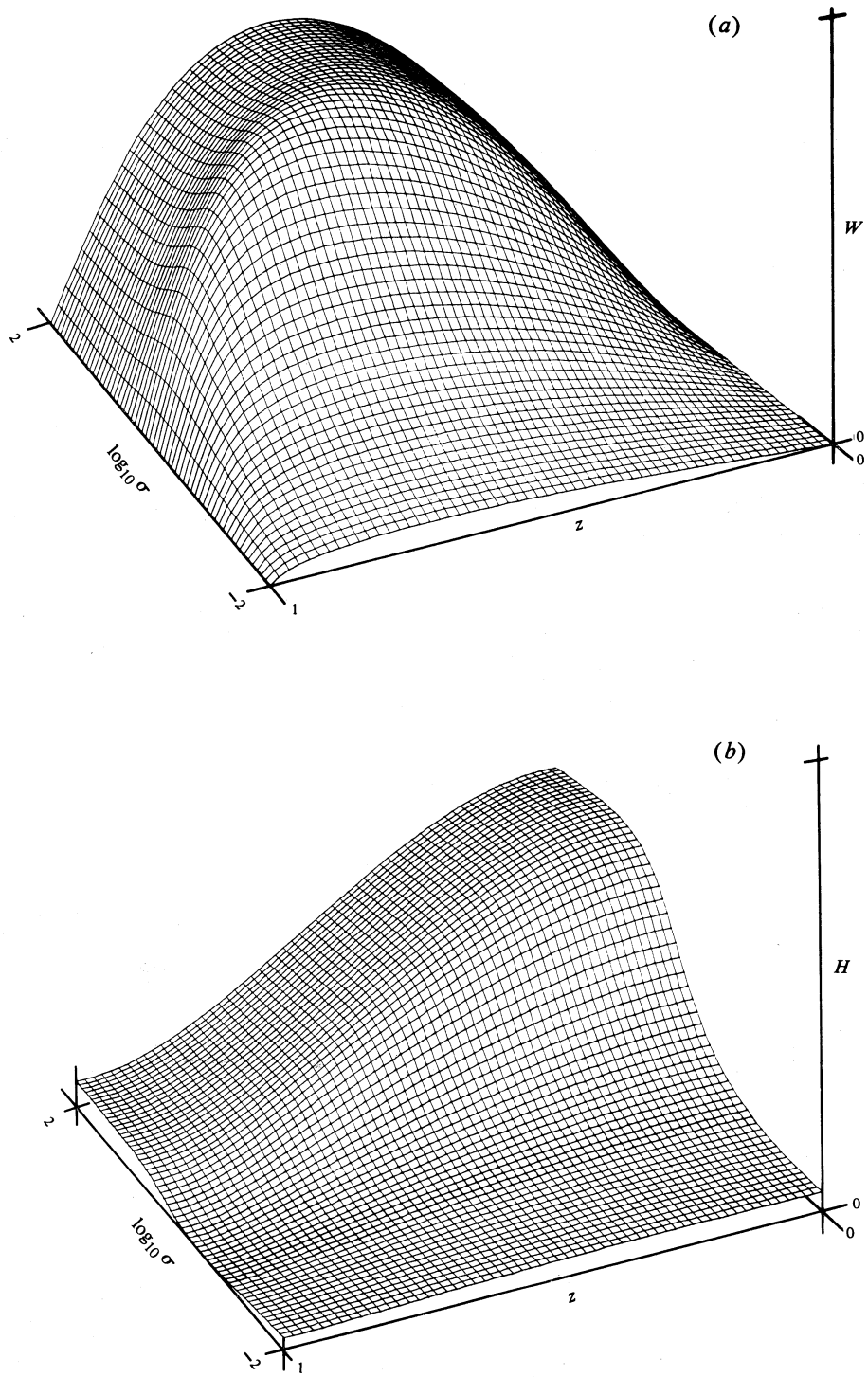

Fig. 11. Profiles over $0 \leqslant z \leqslant 1$ showing the variation with σ of the (*a*) vertical velocity $W(z)$, (*b*) induced vertical magnetic field $H(z)$, (*c*) temperature fluctuation $F(z)$ and (*d*) mean temperature $T_0(z)$, for $R = 3 \times 10^4$, $Q = 10$, $\tau = 10$ and $a = 2{\cdot}63$.

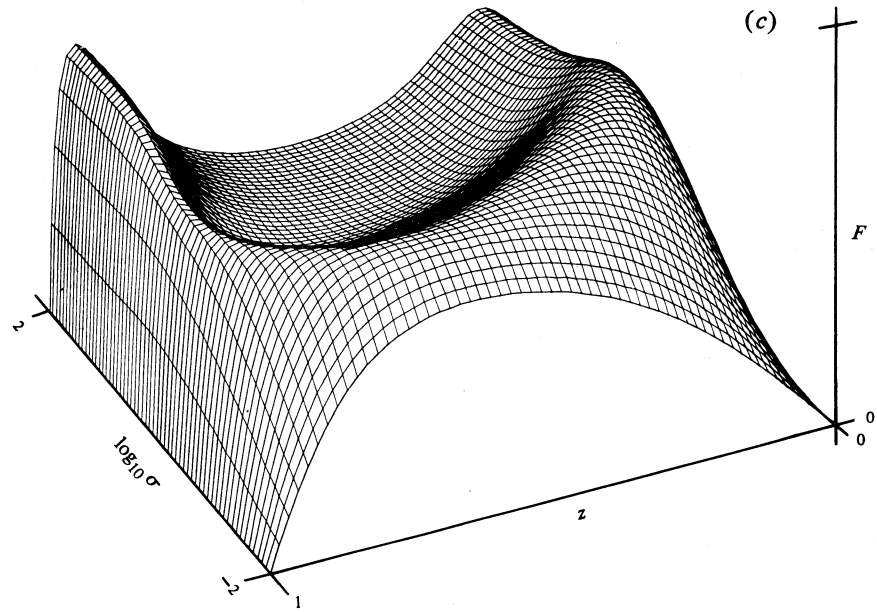

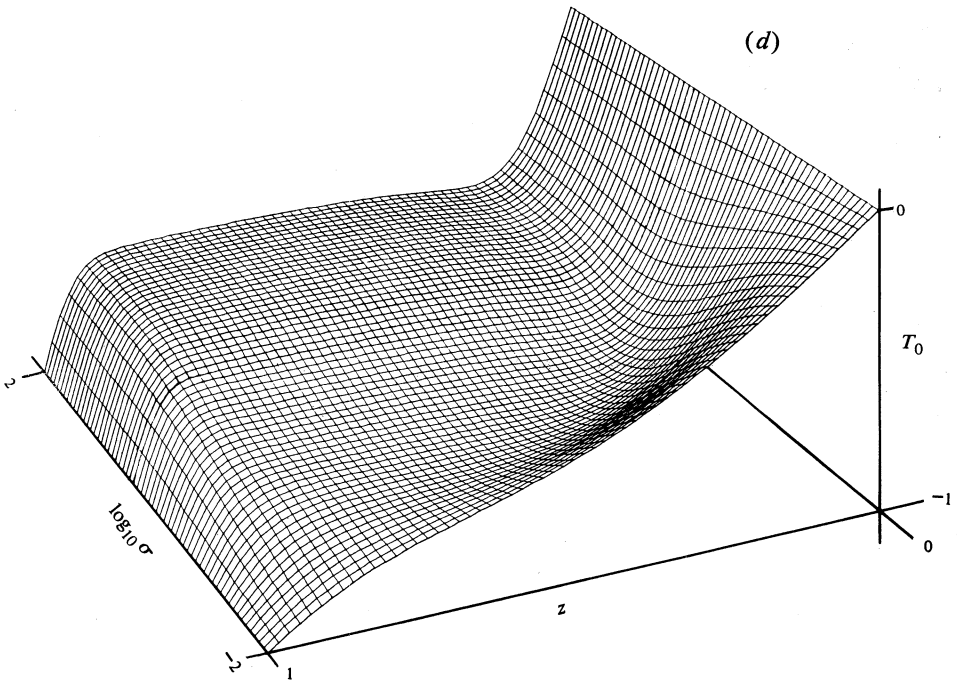

Figs 11*c* and 11*d*.

diffusivities play a much more significant role in the dynamic model presented, and it is the relative values of the diffusivities which determine the extent to which the dynamic terms (e.g. the Lorentz force) dominate in the system.

From the linear theory (Chandrasekhar 1961) it is well known that, depending on the relative values of the diffusivities, the onset of magnetoconvective instabilities may be via an oscillatory bifurcation. It is apparent that a study of time-dependent hexagonal magnetoconvection is warranted as a natural extension of the model presented here.

The question of non-uniqueness of the solution is one that is clearly very difficult to resolve, and the basis of which certainly requires further consideration. The nature of the boundary conditions chosen could also be significant in possibly eliminating the existence of these newly found solutions.

References

Chandrasekhar, S. (1961). 'Hydrodynamic and Hydromagnetic Stability' (Oxford Univ. Press).
Danielson, R. E. (1961). *Astrophys. J.* **134**, 289.
Galloway, D. J., and Proctor, M. R. E. (1983). *Geophys. Astrophys. Fluid Dyn.* **24**, 109.
Galloway, D. J., and Weiss, N. O. (1981). *Astrophys. J.* **243**, 945.
Golub, L., Rosner, R., Vaiana, G. S., and Weiss, N. O. (1981). *Astrophys. J.* **243**, 309.
Gough, D. O., Spiegel, E. A., and Toomre, J. (1975). *J. Fluid Mech.* **68**, 695.
Knobloch, E. (1981). *Astrophys. J.* **247**, L93.
Knobloch, E., and Rosner, R. (1981). *Astrophys. J.* **247**, 300.
Lopez, J. M., and Murphy, J. O. (1983). *Proc. Astron. Soc. Aust.* **5**, 173.
Lopez, J. M., and Murphy, J. O. (1984). *Aust. J. Phys.* **37**, 531.
Murphy, J. O. (1971). *Proc. Astron. Soc. Aust.* **2**, 53.
Murphy, J. O., and Lopez, J. M. (1984). *Aust. J. Phys.* **37**, 179.
Nakagawa, Y. (1957). *Proc. R. Soc. London* A **242**, 81.
Nakagawa, Y. (1959). *Proc. R. Soc. London* A **249**, 138.
Priest, E. R. (1982). 'Solar Magnetohydrodynamics'; Geophysics and Astrophysics Monographs, Vol. 21 (Reidel: Dordrecht).
Proctor, M. R. E., and Galloway, D. J. (1979). *J. Fluid Mech.* **90**, 273.
Roberts, P. H. (1966). *In* 'Non-equilibrium Thermodynamics, Variational Techniques and Stability' (Eds R. J. Donnelly *et al.*), p. 125 (Chicago Univ. Press).
Toomre, J., Gough, D. O., and Spiegel, E. A. (1982). *J. Fluid Mech.* **125**, 99.
Van der Borght, R., and Murphy, J. O. (1973). *Aust. J. Phys.* **26**, 617.
Van der Borght, R., Murphy, J. O., and Spiegel, E. A. (1972). *Aust. J. Phys.* **25**, 702.
Van der Borght, R., Murphy, J. O., and Steiner, J. M. (1974). *Z. Angew. Math. Mech.* **54**, 1.
Weiss, N. O. (1966). *Proc. R. Soc. London* A **293**, 310.
Weiss, N. O. (1981*a*). *J. Fluid Mech.* **108**, 247.
Weiss, N. O. (1981*b*). *J. Fluid Mech.* **108**, 273.
Weiss, N. O. (1981*c*). *J. Geophys. Res.* **86**, 11, 689.

Manuscript received 1 November 1984, accepted 24 January 1985